Sensor Fusion Based UAV Localisation System for Low Cost Autonomous Inspection in Extremely Confined Environments

Beiya Yang, *Member, IEEE*, Erfu Yang, *Senior Member, IEEE*, Leijian Yu, *Graduate Student Member, IEEE*
and Cong Niu, *Member, IEEE*

***Abstract*— Utilising the unmanned aerial vehicle (UAV) for autonomous inspection in extremely confined environments has become a much sought research area, due to the pressing industrial needs. To provide the high accuracy position information of UAV in such environments, the ultra-wideband (UWB) based localisation technology has been one of the ideal candidates. However, the unpredictable propagation condition and the geomagnetic disturbances for inertial measurement unit (IMU) will all have huge impact on the positioning performance with the single UWB and the IMU/UWB based loosely coupled (LC) sensor fusion approach. Therefore, a tightly coupled adaptive extended Kalman filter (TC-AEKF) based sensor fusion UAV localisation system is proposed and developed in this paper for autonomous inspection in extremely confined environments. The proposed system can attain high accuracy localisation of UAV with 0.097m median error, 0.167m 95th percentile error and 0.039m average standard deviation (STD). The drift led by the geomagnetic disturbances for IMU is greatly reduced with the estimation error of the roll, pitch and yaw angle to be 2.15°, 1.54° and 4.58°, respectively. Finally, an autonomous inspection experiment has been conducted to prove the effectiveness of the proposed system and algorithm for actual application, the video from it has been attached in URL https://youtu.be/nEgvwbIVRRk.**

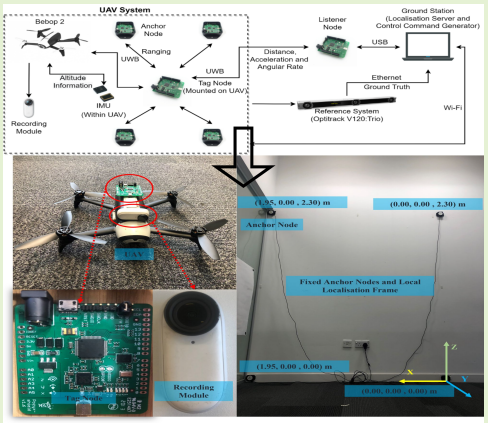

***Index Terms*— Unmanned aerial vehicle (UAV), tightly coupled sensor fusion, autonomous inspection, ultra-wideband (UWB), inertial measurement unit (IMU), extremely confined environments.**

I. Introduction

ALONG with the development of robotic based technologies, the applications for the unmanned aerial vehicle (UAV) based inspection in industry area have become a much sought research area. Currently, lots of researches and commercial solutions have already been made for efficient and detailed inspection with the UAV inside the extremely confined industrial space such as water tank, oil and gas pressure vessel, penstocks and boiler to substitute humans [1]–[5]. In order to do the autonomous and efficient inspection in such environment, the position information for the UAV will be one of the crucial information to be acquired. However, due to the unavailability of the global positioning system (GPS) inside such environments, current systems such as the famous commercial UAV system Elios 2 designed by the Flyability [5] relies on the manually control by the well-trained engineers. This will certainly increase the collision or crash risk and limit the efficiency for the whole system. Therefore, to achieve the autonomous and efficient inspection in extremely confined environments, a new localisation technology is required.

Lots of localisation technologies including visual odometry (VO), light detection and ranging (LiDAR), ultrasonic and ultra-wideband (UWB) have already been investigated for high performance UAV positioning [6]. Among them, the VO is the extensively adopted one, due to the high

This work was partially supported by Research Excellence Award studentship from University of Strathclyde, Low Cost Intelligent UAV Swarming Technology for Visual Inspection project from the UK Net Zero Technology Centre (Grant No. AI-P-028), the MOEA/D-PPR research project (Grant No. IEC-NSFC-211434) funded by the Royal Society. Beiya Yang is now supported in part by the Fundamental Research Funds for the Central Universities (Grant No. D5000230340), National Key Research and Development Program of China (Grant No. SQ2023YFF0900037) and the Key Research and Development Program of Shaanxi (Grant No. 2023-GHZD-42).

Beiya Yang is within the School of Computer Science and Technology, Northwestern Polytechnical University, 127 West Youyi Road, Beilin District, Xi'an Shaanxi, 710072, P.R.China. It needs to note that all the work belongs to Beiya Yang's PhD project which has been carried out and already finished in the UK.

Erfu Yang is within the Department of Design, Manufacturing and Engineering Management, University of Strathclyde, 75 Montrose Street, Glasgow G1 1XJ, UK. The corresponding author is Dr. Erfu Yang. (email: erfu.yang@strath.ac.uk). Leijian Yu and Cong Niu were with the Department of Design, Manufacturing and Engineering Management, University of Strathclyde, 75 Montrose Street, Glasgow G1 1XJ, UK.

accuracy, implementation simplicity, low cost and low prior information requirement characteristics [7]–[9]. However, the low illumination condition for applications in extremely confined environments has the huge impact on the localisation performance. Apart from VO, the LiDAR based technologies have also attracted plenty of attentions on UAV positioning, owing to the enhanced accuracy and robustness features in different environments [10], [11]. Nevertheless, the large weight and high cost for the LiDAR system cannot be ignored for UAV applications. The ultrasonic [12] and UWB [13] are the two positioning technologies with similar localisation principle. These two technologies all leverage the pre-deployed auxiliary nodes for localisation. Yet, even centimetre-level accuracy can be attained with ultrasonic, the low update rate (around 16Hz) led by the inherent nature of the acoustic wave and vulnerable to the unpredictable signal occlusion still restrict its applications on UAV [14]. For the UWB based localisation technologies, high temporal resolution for high accuracy ranging (centimetre-level) can be obtained with the large bandwidth and nanosecond nonsinusoidal narrow pulse transmission signal [15], [16]. The performance impact caused by the signal occlusion between the UWB sensor nodes can also be limited with these characteristics. Moreover, considering the inherent nature of the electromagnetic wave, the performance degradation due to the low illumination conditions can be ignored, and the extremely high signal transmission speed can provide high update rate for the ranging information (around 25Hz according to the real experiment). Therefore, the UWB based localisation technologies can be seen as the ideal candidate for UAV applications in extremely confined environments. However, the potential performance oscillation and degradation caused by the variation of the operational environment and the unpredictable propagation condition between the UWB sensor nodes still exist.

To solve the existing issues, the inertial measurement unit (IMU) and UWB based sensor fusion approach is known as the extensively exploited one. In [17], an extended Kalman filter (EKF) based localisation system was designed through the integration of IMU and the position information from UWB for indoor navigation applications. Meanwhile, Strohmeier et al. [18] proposed an EKF sensor fusion approach with the utilisation of the position information from UWB for UAV localisation. Likely, both the position information from IMU and UWB in [19] was taken into account for position estimation. Since the position information from UWB is the high level information estimated through the original measurements, which is known as the pre-processed information, approaches in [17], [18] and [19] can be seen as the loosely coupled (LC) sensor fusion approach. The performance of these approaches is significantly restricted by the positioning algorithm on the UWB system. Similarly, authors in [15], [20] and [21] were focused on the research about the sensor fusion approach based on IMU and UWB. Differently, they all exploited the low level ranging measurements from the UWB sensor nodes for position estimation. With the directly utilised ranging information, the potential performance degradation caused by the pure UWB based positioning algorithm can be ignored. Yet, the coordinate transformation process of the algorithms in [15] and [20] still rely on the estimated attitude information from IMU, the potential drift for the attitude information caused by the magnetometer in our focused environments still have great impact. To overcome this potential drift, authors in [18] and [21] all introduced the angular rate in the state prediction process for performance improvement. Nevertheless, Strohmeier et al. [18] directly utilised the estimated position information as the observation information which greatly limits the system performance. Both of them have not considered the performance influence caused by the changing environment, they all treated the noise covariance matrices as constant. For the EKF based sensor fusion approach, the two noise covariance matrices which known as the $\boldsymbol{Q}$ and $\boldsymbol{R}$ matrices highly affect the performance [22]–[24]. An inappropriate noise model will directly cause the performance degradation or even the filtering divergence [25]. Furthermore, during the flight of UAV, the variation of the propagation condition for the UWB sensor nodes always exists, which means that even the $\boldsymbol{Q}$ and $\boldsymbol{R}$ matrices can be tuned through trial and error, however, this variation still has great impact on the system performance when these constant noise covariance matrices [26] are utilised. Thus, how to obtain the suitable noise covariance matrices dynamically is the other issue has to be solved urgently. In the authors' previous work [27], the noise covariance matrices have been successfully estimated to deal with the performance influence caused by the variation of the operational environment and the unpredictable propagation condition. Nevertheless, the potential drift for the attitude information caused by the magnetometer still has the great impact on the positioning performance and requires to be resolved.

To remedy all the aforementioned issues, a tightly coupled adaptive extended Kalman filter (TC-AEKF) based sensor fusion approach is proposed. Leveraging the TC sensor fusion approach and the consideration of the angular rate in the process model, the drift on the attitude information caused by the magnetometer on IMU in our focused environments can be eliminated. Meanwhile, with the utilisation of the low level ranging information from UWB, the performance influence from the pure UWB based positioning algorithm can be ignored. Moreover, for the unknown noise covariance matrices, through the proposed AEKF algorithm, these two noise covariance matrices can be adaptively estimated to establish more accurate noise model for performance improvement. To make it clear, the main contributions of this paper are listed:

1) Compared with the traditional LC sensor fusion approach, for the proposed TC-AEKF algorithm, the angular rate is considered in the state prediction process. This is to limit the performance degradation and oscillation caused by the magnetometer on the IMU. With the introduction of the angular rate, the drift for the attitude information can be limited to prevent the performance influence.
2) Considering the performance degradation and oscillation led by the unknown and constant noise covariance matrices, the weighting factor based adaptive estimation approach is introduced in the proposed TC-AEKF algorithm. With the adaptively estimated noise covariance

matrices and the weighting factors, the proposed TC-AEKF algorithm can catch up the changes for the operational environment, get rid of the potential filtering divergence and maintain a high precision localisation performance to keep the stability of the UAV in focused environments. From the evaluation results, it can be proved that the proposed approach significantly elevates the UAV localisation performance in extremely confined environments.

3) A low cost UAV based inspection system is presented and implemented for the autonomous inspection inside extremely confined environments and the evaluation of the proposed localisation approach. According to the real flight tests, the proposed system is capable of the autonomous inspection in extremely confined environments to substitute humans.

In order to show the structure of the system and the whole operational process, the system overview is made in Section II. Then, the detailed description for the proposed algorithm is presented in Section III. Afterwards, for the purpose of comprehensive validation, simulations and experiments including the performance evaluation experiments and the autonomous inspection flight test are conducted and analysed in Section IV. Finally, the conclusion is drawn in Section V.

II. System Overview

The whole UAV system is composed of six modules as depicted in Fig. 1. The commercial low cost quadcopter known as Bebop 2 designed by Parrot is served as the UAV module. The second one is the UWB module. It consists of four fixed anchor nodes (auxiliary nodes with known positions), one tag node (node to be located, containing one IMU module on it to provide the acceleration and angular rate information) attached on UAV and one listener node to communicate with the ground station. In addition, there is another IMU module integrated within the UAV to provide the observation information for the correction of the predicted information. Then is the recording module, known as the Insta360 go 2. It is responsible for the high quality video recording and image capturing. To achieve the UAV stable control, a ground station (laptop) is required for algorithm operation and command generation. Finally is the reference system (OptiTrack V120:Trio) to provide the ground truth for performance evaluation. The price, size and weight for each component are listed in Table I. The cost for the IMU module is already included in the Bebop 2. The cost for the UWB system including one tag node, one listener node, four anchor nodes and relevant accessories. The size and weight for the UWB system in the table represents the size and weight for the tag node, considering only the tag node is equipped on UAV. The reference system is only exploited for the performance evaluation and the ground station does not belong to the UAV system. Therefore, the prices and sizes of these two modules are not considered.

As shown in Fig. 1, the acceleration and angular rate are firstly captured during the operational process. This is done by the gyroscope on the tag node. Then, the captured information is transmitted to the ground station through the listener node for the state prediction. The listener node is directly connected with the ground station through USB cable. Simultaneously, the distance and the attitude information are recorded and calculated by the UWB sensor nodes and the IMU on UAV. Afterwards, these are transmitted to the ground station for the state correction. In the system, the ground station also serves as the localisation server, which is responsible for the operation of the localisation algorithm. Finally, with the predicted and corrected information of UAV, the control command is generated by the ground station. Then it is sent back to the UAV via Wi-Fi for position and attitude control.

TABLE I
SIZE, WEIGHT AND PRICE FOR EACH COMPONENT.

Name	Price (£)	Size (mm)	Weight (g)
Parrot Bebop 2	279.99	381 × 327.7 × 88.9	504
UWB System	583	60 × 53 × 1	12
Insta 360 go 2	294.99	52.9 × 23.6 × 20.7	26.5

III. Sensor Fusion Based UAV Positioning

In order to solve the existing issues for the current single UWB based localisation system and the traditional LC sensor fusion approach, a novel TC-AEKF sensor fusion approach is proposed and introduced in this section.

A. Transformation of the coordinate system

In the proposed system, different from traditional applications, the local coordinate system is determined by four fixed anchor nodes, which is denoted as $OX_{UWB}Y_{UWB}Z_{UWB}$. Apart from the local coordinate system, the acceleration, angular rate and attitude information of UAV are all based on the body frame of UAV which is noted as $OX_BY_BZ_B$. Therefore, for the purpose of the position estimation through the measured acceleration information, the conversion between these two coordinate systems is required.

The whole conversion process can be divided into three steps. Firstly, transforming the acceleration information from the UAV body frame into the pitch frame with the estimated roll angle ϕ from the TC-AEKF approach is made. Then, leveraging the same principle, converting the acceleration information in the pitch frame into the yaw frame with the estimated pitch angle θ is conducted. Finally, utilising the estimated yaw angle ψ, rotating it into the local coordinate system determined by the fixed anchor nodes is made. The whole transformation process can be described as

$$\boldsymbol{a}^{UWB} = \begin{bmatrix} \cos\psi\cos\theta & a_{12} & a_{13} \\ \cos\theta\sin\psi & a_{22} & a_{23} \\ -\sin\theta & \cos\theta\sin\phi & \cos\theta\cos\phi \end{bmatrix} \boldsymbol{a}^{B}, \quad (1)$$

where, $\boldsymbol{a}^B$ is the measured acceleration information in the body frame,

$$\boldsymbol{C}^{BUWB} = \begin{bmatrix} \cos\psi\cos\theta & a_{12} & a_{13} \\ \cos\theta\sin\psi & a_{22} & a_{23} \\ -\sin\theta & \cos\theta\sin\phi & \cos\theta\cos\phi \end{bmatrix}, \quad (2)$$

is the transformation matrix, $\boldsymbol{a}^{UWB}$ denotes the transformation results which is known as the acceleration information

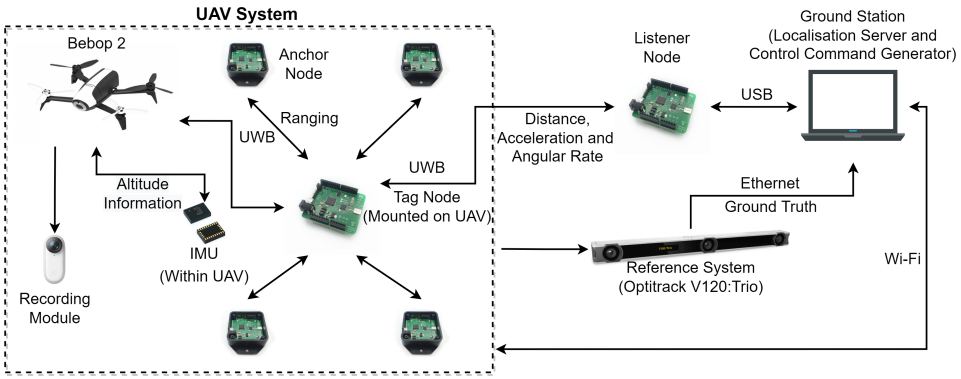

Fig. 1. System structure.

in the local frame, $a_{12} = \cos\psi\sin\theta\sin\phi - \cos\phi\sin\psi$, $a_{13} = \sin\psi\sin\phi + \cos\psi\cos\phi\sin\theta$, $a_{22} = \cos\psi\cos\phi + \sin\psi\sin\theta\sin\phi$, $a_{23} = \cos\phi\sin\psi\sin\theta - \cos\psi\sin\phi$.

B. TC-AEKF based sensor fusion approach

1) State prediction process: Throughout the UAV kinematic model [28], the state transition equation can be represented as

$$\begin{cases} \hat{\boldsymbol{\gamma}}_{k/k-1} = \boldsymbol{\gamma}_{k-1} + \Delta T\boldsymbol{\omega}_{k-1} \\ \hat{\boldsymbol{p}}_{k/k-1} = \boldsymbol{p}_{k-1} + \Delta T\boldsymbol{v}_{k-1} + \frac{\Delta T^2}{2}\boldsymbol{a}_{k-1}^{UWB} \\ \hat{\boldsymbol{v}}_{k/k-1} = \boldsymbol{v}_{k-1} + \Delta T\boldsymbol{a}_{k-1}^{UWB} \\ \boldsymbol{a}_{k-1}^{UWB} = \boldsymbol{C}_{k-1}^{BUWB}\boldsymbol{a}_{k-1}^{B} \end{cases}, \tag{3}$$

where, $\boldsymbol{\gamma} = [\phi\ \theta\ \psi]^T$ is the attitude of UAV, $\boldsymbol{\omega} = [\omega_\phi\ \omega_\theta\ \omega_\psi]^T$ is the angular rate, $\boldsymbol{p} = [x\ y\ z]^T$ represents the UAV position information, $\boldsymbol{v} = [v_x\ v_y\ v_z]^T$ is the velocity at X, Y and Z direction, $\boldsymbol{a}^{UWB} = [a_x^{UWB}\ a_y^{UWB}\ a_z^{UWB}]^T$ is the acceleration at X, Y and Z direction in local localisation frame, ΔT denotes the time interval between two round measurements. The variables with the subscript $k/k-1$ represent these variables are the intermediate variables between two rounds and are estimated through the prediction process. It is noted here that the acceleration and angular rate between two rounds are assumed as constant. Then, transforming the equation into matrix form yields

$$\begin{bmatrix} \hat{\boldsymbol{\rho}}_{k/k-1} \\ \hat{\boldsymbol{u}}_{k/k-1} \end{bmatrix} = \begin{bmatrix} \boldsymbol{F}_k^{\boldsymbol{\rho}} & \boldsymbol{0} \\ \boldsymbol{0} & \boldsymbol{F}_k^{\boldsymbol{u}} \end{bmatrix} \begin{bmatrix} \boldsymbol{\rho}_{k-1} \\ \boldsymbol{u}_{k-1} \end{bmatrix} + \begin{bmatrix} \boldsymbol{0} & \boldsymbol{0} \\ \boldsymbol{0} & \boldsymbol{B}_k^{\boldsymbol{u}} \end{bmatrix} \begin{bmatrix} \boldsymbol{0} \\ \boldsymbol{a}_{k-1}^{UWB} \end{bmatrix}, \tag{4}$$

in which, $\boldsymbol{\rho} = [\phi\ \omega_\phi\ \theta\ \omega_\theta\ \psi\ \omega_\psi]^T$ represents the UAV attitude and angular rate information, $\boldsymbol{u} = [x\ v_x\ y\ v_y\ z\ v_z]^T$ consists of the position and velocity information in this round, the state transition matrix is composed of $\boldsymbol{F}_k^{\boldsymbol{\rho}}$ and $\boldsymbol{F}_k^{\boldsymbol{u}}$,

$$\boldsymbol{F}_k^{\boldsymbol{\rho}} = \boldsymbol{F}_k^{\boldsymbol{u}} = \boldsymbol{I}_3 \otimes \begin{bmatrix} 1 & \Delta T \\ 0 & 1 \end{bmatrix}, \tag{5}$$

the control matrix is constituted by $\boldsymbol{B}_k^{\boldsymbol{u}}$,

$$\boldsymbol{B}_k^{\boldsymbol{u}} = \boldsymbol{I}_3 \otimes \begin{bmatrix} \frac{\Delta T^2}{2} \\ \Delta T \end{bmatrix}, \tag{6}$$

where, $\boldsymbol{I}$ represents the identity matrix, "$\otimes$" is the Kronecker product.

In the actual process, the measurement noise and gyro bias for the measured information including the angular rate and acceleration should be considered and represented as follows,

$$\boldsymbol{\omega} = \tilde{\boldsymbol{\omega}} + \boldsymbol{b}^{\omega} + \boldsymbol{e}, \tag{7}$$

$$\boldsymbol{a}^{UWB} = \tilde{\boldsymbol{a}}^{UWB} + \boldsymbol{b}^{a} + \boldsymbol{n}. \tag{8}$$

Where, corresponding to the literatures in [21], [29] all the measurement noise and the gyro bias are modelled as the additive white Gaussian noise (AWGN) with zero mean and variance. These are listed as, $\boldsymbol{b}^{\omega} \sim N(\boldsymbol{0}, \boldsymbol{\sigma}_{b\omega}^2)$, $\boldsymbol{b}^{a} \sim N(\boldsymbol{0}, \boldsymbol{\sigma}_{ba}^2)$, $\boldsymbol{e} \sim N(\boldsymbol{0}, \boldsymbol{\sigma}_{e}^2)$ and $\boldsymbol{n} \sim N(\boldsymbol{0}, \boldsymbol{\sigma}_{n}^2)$. $\tilde{\boldsymbol{\omega}}$ and $\tilde{\boldsymbol{a}}^{UWB}$ are assumed as the true value of the angular rate and acceleration. $\boldsymbol{\omega}$ and $\boldsymbol{a}^{UWB}$ are supposed to be the measured value of them. Then, from (4), (7) and (8), the state covariance matrix can be derived

$$\begin{aligned} \hat{\boldsymbol{A}}_{k/k-1} = &\begin{bmatrix} \boldsymbol{F}_k^{\boldsymbol{\rho}} & \boldsymbol{0} \\ \boldsymbol{0} & \boldsymbol{F}_k^{\boldsymbol{u}} \end{bmatrix} \begin{bmatrix} \boldsymbol{\rho}_{k-1} \\ \boldsymbol{u}_{k-1} \end{bmatrix} \begin{bmatrix} \boldsymbol{\rho}_{k-1} \\ \boldsymbol{u}_{k-1} \end{bmatrix}^T \begin{bmatrix} \boldsymbol{F}_k^{\boldsymbol{\rho}} & \boldsymbol{0} \\ \boldsymbol{0} & \boldsymbol{F}_k^{\boldsymbol{u}} \end{bmatrix}^T \\ &+ \begin{bmatrix} \boldsymbol{Q}_k^{\boldsymbol{\rho}} + \boldsymbol{Q}_k^{\boldsymbol{b}^{\omega}} & \boldsymbol{0} \\ \boldsymbol{0} & \boldsymbol{Q}_k^{\boldsymbol{u}} + \boldsymbol{Q}_k^{\boldsymbol{b}^{a}} \end{bmatrix}, \end{aligned} \tag{9}$$

where, the state process noise covariance matrix $\boldsymbol{Q}$ is constituted by the noise and bias from IMU measurements, $\boldsymbol{Q}_k^{\boldsymbol{\rho}} = \boldsymbol{F}_k^{\boldsymbol{\rho}}\boldsymbol{e}_k\boldsymbol{e}_k{}^T\boldsymbol{F}_k^{\boldsymbol{\rho}T}$, $\boldsymbol{Q}_k^{\boldsymbol{b}^{\omega}} = \boldsymbol{F}_k^{\boldsymbol{\rho}}\boldsymbol{b}_k^{\omega}\boldsymbol{b}_k^{\omega T}\boldsymbol{F}_k^{\boldsymbol{\rho}T}$, $\boldsymbol{Q}_k^{\boldsymbol{u}} = \boldsymbol{B}_k^{\boldsymbol{u}}\boldsymbol{n}_k\boldsymbol{n}_k^T\boldsymbol{B}_k^{\boldsymbol{u}T}$ and $\boldsymbol{Q}_k^{\boldsymbol{b}^{a}} = \boldsymbol{B}_k^{\boldsymbol{u}}\boldsymbol{b}_k^{a}\boldsymbol{b}_k^{a\,T}\boldsymbol{B}_k^{\boldsymbol{u}T}$.

Then, the position and attitude information of UAV can be predicted. However, in the actual process, the cumulative error always exists which will directly cause the performance degradation as time goes on. Therefore, a correction process to update the predicted information is required.

2) Correction process: In the system, the precise distance information between the tag node and fixed anchor nodes can be obtained through the communication within these UWB sensor nodes. To prevent the requirement of the strict time synchronisation between these nodes, the two-way time of flight (TW-TOF) ranging scheme is selected. For the TW-TOF, with the measured time of departure (TOD) and time of arrival (TOA) information on each side, the clock difference between these nodes can be cancelled directly. Then, the measured distance information from TW-TOF is served as the observation information to correct and update the predicted position information. Moreover, the attitude information provided by the IMU module equipped on the UAV is exploited as the attitude observation information for correction.

Assuming the attitude measurement matrix and the distance measurement matrix at k round to be $\boldsymbol{\zeta}_k^{\boldsymbol{\rho}}$ and $\boldsymbol{\zeta}_k^{\boldsymbol{u}}$, the observation equation can be derived as

$$\begin{bmatrix}\boldsymbol{\zeta}_k^{\boldsymbol{\rho}}\\ \boldsymbol{\zeta}_k^{\boldsymbol{u}}\end{bmatrix} = \begin{bmatrix}\boldsymbol{H}_k^{\boldsymbol{\rho}} & \mathbf{0}\\ \mathbf{0} & \boldsymbol{H}_k^{\boldsymbol{u}}\end{bmatrix}\begin{bmatrix}\hat{\boldsymbol{\rho}}_{k/k-1}\\ \hat{\boldsymbol{u}}_{k/k-1}\end{bmatrix} + \begin{bmatrix}\boldsymbol{\epsilon}_k\\ \boldsymbol{\eta}_k\end{bmatrix}, \tag{10}$$

in which, the observation transition matrix is composed of $\boldsymbol{H}_k^{\boldsymbol{\rho}}$ and $\boldsymbol{H}_k^{\boldsymbol{u}}$, $\boldsymbol{\epsilon} \sim N(\mathbf{0}, \boldsymbol{\sigma}_\epsilon^2)$ and $\boldsymbol{\eta} \sim N(\mathbf{0}, \boldsymbol{\sigma}_\eta^2)$ are denoted as the attitude measurement noise and distance measurement noise which are all modelled as the AWGN. Considering that the observation information $\boldsymbol{\zeta}_k^{\boldsymbol{\rho}}$ measured from the IMU is the attitude, the transition matrix $\boldsymbol{H}_k^{\boldsymbol{\rho}}$ can be

$$\boldsymbol{H}_k^{\boldsymbol{\rho}} = \begin{bmatrix}1 & 0 & 0 & 0 & 0 & 0\\ 0 & 0 & 1 & 0 & 0 & 0\\ 0 & 0 & 0 & 0 & 1 & 0\end{bmatrix}. \tag{11}$$

Differently, $\boldsymbol{\zeta}_k^{\boldsymbol{u}}$ measured by the UWB sensor nodes is the distance information, therefore, a conversion is required. Since the distance information cannot be linearly represented by the position information, the first order Taylor expansion is utilised,

$$\boldsymbol{H}_k^{\boldsymbol{u}} = \begin{bmatrix}\frac{\partial d_{1,k/k-1}}{\partial \hat{x}_{k/k-1}} & 0 & \frac{\partial d_{1,k/k-1}}{\partial \hat{y}_{k/k-1}} & 0 & \frac{\partial d_{1,k/k-1}}{\partial \hat{z}_{k/k-1}} & 0\\ \frac{\partial d_{2,k/k-1}}{\partial \hat{x}_{k/k-1}} & 0 & \frac{\partial d_{2,k/k-1}}{\partial \hat{y}_{k/k-1}} & 0 & \frac{\partial d_{2,k/k-1}}{\partial \hat{z}_{k/k-1}} & 0\\ \vdots & \vdots & \vdots & \vdots & \vdots & \vdots\\ \frac{\partial d_{j,k/k-1}}{\partial \hat{x}_{k/k-1}} & 0 & \frac{\partial d_{j,k/k-1}}{\partial \hat{y}_{k/k-1}} & 0 & \frac{\partial d_{j,k/k-1}}{\partial \hat{z}_{k/k-1}} & 0\end{bmatrix}, \tag{12}$$

where, j is supposed to be the number of fixed anchor nodes.

The Kalman gain can be obtained throughout the aforementioned processes and represented by

$$\begin{aligned}\boldsymbol{K}_{gain} =& \hat{\boldsymbol{A}}_{k/k-1}\begin{bmatrix}\boldsymbol{H}_k^{\boldsymbol{\rho}} & \mathbf{0}\\ \mathbf{0} & \boldsymbol{H}_k^{\boldsymbol{u}}\end{bmatrix}^T\\ &\cdot\Big(\begin{bmatrix}\boldsymbol{H}_k^{\boldsymbol{\rho}} & \mathbf{0}\\ \mathbf{0} & \boldsymbol{H}_k^{\boldsymbol{u}}\end{bmatrix}\hat{\boldsymbol{A}}_{k/k-1}\begin{bmatrix}\boldsymbol{H}_k^{\boldsymbol{\rho}} & \mathbf{0}\\ \mathbf{0} & \boldsymbol{H}_k^{\boldsymbol{u}}\end{bmatrix}^T\\ &+\begin{bmatrix}\boldsymbol{R}_k^{\boldsymbol{\rho}} & \mathbf{0}\\ \mathbf{0} & \boldsymbol{R}_k^{\boldsymbol{u}}\end{bmatrix}\Big)^{-1},\end{aligned} \tag{13}$$

where, the combination of $\boldsymbol{R}_k^{\boldsymbol{\rho}}$ and $\boldsymbol{R}_k^{\boldsymbol{u}}$ is supposed to be the measurement noise covariance matrix $\boldsymbol{R}$.

Finally, the position and attitude information from the prediction process can be corrected, i.e.

$$\begin{aligned}\begin{bmatrix}\hat{\boldsymbol{\rho}}_k\\ \hat{\boldsymbol{u}}_k\end{bmatrix} =& \begin{bmatrix}\hat{\boldsymbol{\rho}}_{k/k-1}\\ \hat{\boldsymbol{u}}_{k/k-1}\end{bmatrix}\\ &+\boldsymbol{K}_{gain}\Big(\begin{bmatrix}\boldsymbol{\zeta}_k^{\boldsymbol{\rho}}\\ \boldsymbol{\zeta}_k^{\boldsymbol{u}}\end{bmatrix} - \begin{bmatrix}\boldsymbol{H}_k^{\boldsymbol{\rho}} & \mathbf{0}\\ \mathbf{0} & \boldsymbol{H}_k^{\boldsymbol{u}}\end{bmatrix}\begin{bmatrix}\hat{\boldsymbol{\rho}}_{k/k-1}\\ \hat{\boldsymbol{u}}_{k/k-1}\end{bmatrix}\Big),\end{aligned} \tag{14}$$

$$\hat{\boldsymbol{A}}_k = \hat{\boldsymbol{A}}_{k/k-1} - \boldsymbol{K}_{gain}\begin{bmatrix}\boldsymbol{H}_k^{\boldsymbol{\rho}} & \mathbf{0}\\ \mathbf{0} & \boldsymbol{H}_k^{\boldsymbol{u}}\end{bmatrix}\hat{\boldsymbol{A}}_{k/k-1}. \tag{15}$$

3) Observability analysis: In order to prove the effectiveness of the proposed algorithm and system, the observability analysis has been done as follows. Considering the linearisation for the observation transition matrix has already been done in the previous process, the piecewise constant system (PWCS) method is utilised for analysis. With the state prediction equation in (4), the observation correction equation in (10) and the PWCS method, the total observability matrix (TOM) $\boldsymbol{Q}_k^{\boldsymbol{TOM}}$ for the system can be represented as

$$\boldsymbol{Q}_k^{\boldsymbol{TOM}} = \begin{bmatrix}\boldsymbol{H}_1\\ \boldsymbol{H}_1\boldsymbol{F}_1\\ \cdots\\ \boldsymbol{H}_1\boldsymbol{F}_1^{i-1}\\ \begin{bmatrix}\boldsymbol{H}_2\\ \boldsymbol{H}_2\boldsymbol{F}_2\\ \cdots\\ \boldsymbol{H}_2\boldsymbol{F}_2^{i-1}\\ \cdots\end{bmatrix}\boldsymbol{F}_1^{i-1}\\ \cdots\\ \begin{bmatrix}\boldsymbol{H}_k\\ \boldsymbol{H}_k\boldsymbol{F}_k\\ \cdots\\ \boldsymbol{H}_k\boldsymbol{F}_k^{i-1}\\ \cdots\end{bmatrix}\boldsymbol{F}_{k-1}^{i-1}\boldsymbol{F}_{k-2}^{i-1}\cdots\boldsymbol{F}_1^{i-1}\end{bmatrix}. \tag{16}$$

Within the equation, i is supposed as the number of the state, which is 12 for this system. $\boldsymbol{H}_k$ and $\boldsymbol{F}_k$ is the observation transition matrix and the state transition matrix,

$$\boldsymbol{H}_k = \begin{bmatrix}\boldsymbol{H}_k^{\boldsymbol{\rho}} & \mathbf{0}\\ \mathbf{0} & \boldsymbol{H}_k^{\boldsymbol{u}}\end{bmatrix}, \tag{17}$$

$$\boldsymbol{F}_k = \begin{bmatrix}\boldsymbol{F}_k^{\boldsymbol{\rho}} & \mathbf{0}\\ \mathbf{0} & \boldsymbol{F}_k^{\boldsymbol{u}}\end{bmatrix}. \tag{18}$$

According to the definition of each, it can be proved that the rank of $\boldsymbol{Q}_k^{\boldsymbol{TOM}}$ is 12, which is the same as the number of the state in this system. Thus, the system is observable.

4) Estimation of the noise covariance matrices: Even the precise attitude and position information of the UAV can be attained, nevertheless, how to adjust or decide the $\boldsymbol{Q}$ and $\boldsymbol{R}$ matrices still have huge impact on the localisation performance. Thus, the AEKF based approach is investigated in this section to adptively estimate these matrices for performance improvement [22], [23], [30].

It can be observed that, through (10), the measurement noises can be approximated by the measured and the predicted information in this round,

$$\begin{bmatrix}\boldsymbol{\zeta}_k^{\boldsymbol{\rho}\prime}\\ \boldsymbol{\zeta}_k^{\boldsymbol{u}\prime}\end{bmatrix} = \begin{bmatrix}\boldsymbol{\zeta}_k^{\boldsymbol{\rho}}\\ \boldsymbol{\zeta}_k^{\boldsymbol{u}}\end{bmatrix} - \begin{bmatrix}\boldsymbol{H}_k^{\boldsymbol{\rho}} & \mathbf{0}\\ \mathbf{0} & \boldsymbol{H}_k^{\boldsymbol{u}}\end{bmatrix}\begin{bmatrix}\hat{\boldsymbol{\rho}}_{k/k-1}\\ \hat{\boldsymbol{u}}_{k/k-1}\end{bmatrix}. \tag{19}$$

Therefore, the innovation covariance matrix $\hat{\boldsymbol{C}}_{\boldsymbol{\zeta}_k^{\boldsymbol{\rho}\prime}\boldsymbol{\zeta}_k^{\boldsymbol{u}\prime}}$ can be derived as

$$\hat{\boldsymbol{C}}_{\boldsymbol{\zeta}_k^{\boldsymbol{\rho}\prime}\boldsymbol{\zeta}_k^{\boldsymbol{u}\prime}} = \frac{1}{M}\sum_{i=k-M+1}^{k}\begin{bmatrix}\boldsymbol{\zeta}_i^{\boldsymbol{\rho}\prime}\\ \boldsymbol{\zeta}_i^{\boldsymbol{u}\prime}\end{bmatrix}\begin{bmatrix}\boldsymbol{\zeta}_i^{\boldsymbol{\rho}\prime}\\ \boldsymbol{\zeta}_i^{\boldsymbol{u}\prime}\end{bmatrix}^T, \tag{20}$$

where, M is the sampling number or window size. Then, the estimation of $\boldsymbol{R}$ matrix can be obtained through (19) and (20)

$$\begin{bmatrix}\boldsymbol{R}_k^{\boldsymbol{\rho}} & \mathbf{0}\\ \mathbf{0} & \boldsymbol{R}_k^{\boldsymbol{u}}\end{bmatrix} = \hat{\boldsymbol{C}}_{\boldsymbol{\zeta}_k^{\boldsymbol{\rho}\prime}\boldsymbol{\zeta}_k^{\boldsymbol{u}\prime}} - \begin{bmatrix}\boldsymbol{H}_k^{\boldsymbol{\rho}} & \mathbf{0}\\ \mathbf{0} & \boldsymbol{H}_k^{\boldsymbol{u}}\end{bmatrix}\hat{\boldsymbol{A}}_k\begin{bmatrix}\boldsymbol{H}_k^{\boldsymbol{\rho}} & \mathbf{0}\\ \mathbf{0} & \boldsymbol{H}_k^{\boldsymbol{u}}\end{bmatrix}^T. \tag{21}$$

Similarly, the $\boldsymbol{Q}$ matrix can also be approximated as

$$\begin{bmatrix}\boldsymbol{F}_k^{\boldsymbol{\rho}}\boldsymbol{e}_k + \boldsymbol{F}_k^{\boldsymbol{\rho}}\boldsymbol{b}_k^{\boldsymbol{\omega}}\\ \boldsymbol{B}_k^{\boldsymbol{u}}\boldsymbol{n}_k + \boldsymbol{B}_k^{\boldsymbol{u}}\boldsymbol{b}_k^{\boldsymbol{a}}\end{bmatrix} = \boldsymbol{K}_{gain}\cdot\Big(\begin{bmatrix}\boldsymbol{\zeta}_k^{\boldsymbol{\rho}}\\ \boldsymbol{\zeta}_k^{\boldsymbol{u}}\end{bmatrix} - \begin{bmatrix}\boldsymbol{H}_k^{\boldsymbol{\rho}} & \mathbf{0}\\ \mathbf{0} & \boldsymbol{H}_k^{\boldsymbol{u}}\end{bmatrix}\begin{bmatrix}\hat{\boldsymbol{\rho}}_{k/k-1}\\ \hat{\boldsymbol{u}}_{k/k-1}\end{bmatrix}\Big), \tag{22}$$

$$\begin{bmatrix} \boldsymbol{Q}_k^{\boldsymbol{\rho}} + \boldsymbol{Q}_k^{\boldsymbol{b}^{\omega}} & \mathbf{0} \\ \mathbf{0} & \boldsymbol{Q}_k^{\boldsymbol{u}} + \boldsymbol{Q}_k^{\boldsymbol{b}^{a}} \end{bmatrix} = \boldsymbol{K}_{gain} \hat{\boldsymbol{C}}_{\boldsymbol{\zeta}_k^{\rho\prime} \boldsymbol{\zeta}_k^{\boldsymbol{u}\prime}} \boldsymbol{K}_{gain}^T. \quad (23)$$

However, the estimation of the $\boldsymbol{R}$ and $\boldsymbol{Q}$ matrix still rely on the measured information which may result in the performance oscillation or filtering divergence due to the unpredictable propagation condition between the UWB sensor nodes and the changing operational environment. For traditional positioning applications, such as personnel positioning or object positioning, as the performance oscillation is not a persistent performance degradation, the influence can be safely neglected. Nevertheless, the situation has changed for UAV applications. Since the UAV will react every estimated position information from the system, this performance oscillation may cause the instability of the UAV, especially in the extremely confined environments. Therefore, it is still required to avoid this performance oscillation for the improvement of the UAV stability in such environment. To remedy the existing issue, additional weighting factors are added in the approximation process to limit the estimation of these two noise covariance matrices.

5) Additional weighting factors: Inspired by the estimation approach in [30] and in order to eliminate the performance degradation and prevent the potential filtering divergence. Four weighting factors α, α', β and β', plus with the offline data for these two noise covariance matrices $\boldsymbol{R}_{off}$ and $\boldsymbol{Q}_{off}$ estimated before the flight of UAV are introduced in the approximation process.

Firstly, for the estimation of the measurement noise covariance matrix, with the additional weighting factors α and α', the offline data $\boldsymbol{R}_{off}$ and the approximation equation from (21), it can be derived that

$$\begin{aligned} \boldsymbol{R}_{update} = &\begin{bmatrix} (1-\alpha')\boldsymbol{R}_{off}^{\boldsymbol{\rho}} & \mathbf{0} \\ \mathbf{0} & (1-\alpha)\boldsymbol{R}_{off}^{\boldsymbol{u}} \end{bmatrix} + \begin{bmatrix} \alpha' \\ \alpha \end{bmatrix} \\ &\cdot (\hat{\boldsymbol{C}}_{\boldsymbol{\zeta}_k^{\rho\prime} \boldsymbol{\zeta}_k^{\boldsymbol{u}\prime}} - \begin{bmatrix} \boldsymbol{H}_k^{\boldsymbol{\rho}} & \mathbf{0} \\ \mathbf{0} & \boldsymbol{H}_k^{\boldsymbol{u}} \end{bmatrix} \hat{\boldsymbol{A}}_k \begin{bmatrix} \boldsymbol{H}_k^{\boldsymbol{\rho}} & \mathbf{0} \\ \mathbf{0} & \boldsymbol{H}_k^{\boldsymbol{u}} \end{bmatrix}^T). \end{aligned} \quad (24)$$

Apparently from (24), with the increasing of α and α', more trust is given to the current measurements to catch up the changes caused by the changing environment or propagation condition. However, this may lead to the oscillation for the estimation of the $\boldsymbol{R}$ matrix, which means the filtering divergence is more likely to happen. In contrast, the estimation of the $\boldsymbol{R}$ matrix is relatively stable, but the system needs more time to catch up the changes, which means a long time performance degradation.

Same as the estimation of the $\boldsymbol{R}$ matrix, the other two weighting factors β and β' are added in the estimation of the $\boldsymbol{Q}$ matrix to avoid the performance degradation and filtering divergence. The estimation equation is written as

$$\begin{aligned} \boldsymbol{Q}_{update} = &\begin{bmatrix} (1-\beta')\boldsymbol{Q}_{off}^{\boldsymbol{\rho}} & \mathbf{0} \\ \mathbf{0} & (1-\beta)\boldsymbol{Q}_{off}^{\boldsymbol{u}} \end{bmatrix} \\ &+ \begin{bmatrix} \beta' \\ \beta \end{bmatrix} \boldsymbol{K}_{gain} \hat{\boldsymbol{C}}_{\boldsymbol{\zeta}_k^{\rho\prime} \boldsymbol{\zeta}_k^{\boldsymbol{u}\prime}} \boldsymbol{K}_{gain}^T. \end{aligned} \quad (25)$$

Similarly, with the augmentation of β and β', the estimation of the $\boldsymbol{Q}$ matrix more relies on the current measurements (acceleration and angular rate) to catch up the changes. Otherwise, greater proportion is given to the offline data to keep the estimation process relatively stable, but more time is required to catch up the changes.

Even with the additional weighting factors the estimation performance can be improved, nevertheless, the value of these weighting factors still have huge impact on the localisation performance. To overcome this, an adaptive estimation process is proposed for the estimation of these weighting factors.

Because α and α' are added to limit the estimation of the measurement noise covariance matrix, α and α' can be made through the difference between the current observation information and the predicted information

$$\begin{bmatrix} \alpha'_{ad} \\ \alpha_{ad} \end{bmatrix} = \begin{bmatrix} \frac{\frac{1}{3}\sum_{i=1}^{3}[\boldsymbol{\zeta}_k^{\boldsymbol{\rho}\prime}]_{i1}}{\boldsymbol{\zeta}_{in}^{\boldsymbol{\rho}\prime}} \\ \frac{\frac{1}{j}\sum_{i=1}^{j}[\boldsymbol{\zeta}_k^{\boldsymbol{u}\prime}]_{i1}}{\boldsymbol{\zeta}_{in}^{\boldsymbol{u}\prime}} \end{bmatrix} \begin{bmatrix} \alpha'_{in} \\ \alpha_{in} \end{bmatrix}, \quad (26)$$

where, α_{ad} and α'_{ad} are the adaptively estimated weighting factors, α_{in} and α'_{in} are the initial value for each, $\boldsymbol{\zeta}_{in}^{\boldsymbol{\rho}\prime}$ and $\boldsymbol{\zeta}_{in}^{\boldsymbol{u}\prime}$ represent the initial value for the current difference which are measured through a set of observation and prediction information before the flight of UAV and j is the number of fixed anchor nodes in the system. The number of the fixed anchor nodes will highly affect the system performance. As with the lesser fixed anchor nodes, the number of the observation information (ranging information) may be insufficient to guarantee the high system performance. When more fixed anchor nodes are used, the increased number of the observation information can improve the system performance. However, this is at the expense of decreasing the position update rate. With more fixed anchor nodes, the communication burden for the tag node on the UAV will be increased, which will directly lead to the decreasing of the position update rate. On the other hand, considering the applications are within the extremely confined environments, more anchor nodes applied will also increase the deployment difficulty and limit the application scenarios of the system. Under such circumstance, in this system the number of the fixed anchor nodes is set as 4. Clearly, when the difference between the current observation information and the predicted value becomes larger, α_{ad} and α'_{ad} will also become larger to overtake the current changes. On the contrary, α_{ad} and α'_{ad} will be smaller to give more trust to the offline data to maintain a steady state. Here it needs to note that, in order to avoid the filtering divergence, α_{ad} is set within $0 \leq \alpha_{ad} \leq 0.5$, α_{in} is supposed as 0.5, and α'_{ad} is set within $0 \leq \alpha'_{ad} \leq 0.1$, α'_{in} is set to be 0.1. Considering the potential abrupt change for the observed attitude information from IMU in confined environments, a smaller value limitation for the α'_{ad} is selected to prevent the sudden change for the estimated measurement noise covariance. Furthermore, a negative value may be potentially obtained since the estimation of the measurement noise covariance is from two positive definite matrices. To prevent the filtering divergence caused by the negative value, if a negative value for the estimation is detected, the two weighting factors will be directly set to zero.

Based on the same principle, β and β' can also be estimated through the data from the previous process. But differently,

as the time interval ΔT has more impact on the prediction process, with a larger time interval between two rounds acceleration and angular rate, the noises from these information will have more influence on the prediction performance. Therefore, the estimation of β and β' will more rely on the time interval between two round estimations. Throughout the $\boldsymbol{Q}_{off}$ offline data and the average time interval $\Delta T_{average}$ measured before the flight of UAV, the estimation equation can be derived

$$\begin{bmatrix} \beta'_{ad} \\ \beta_{ad} \end{bmatrix} = \frac{\Delta T}{\Delta T_{average}} \begin{bmatrix} \beta'_{in} \\ \beta_{in} \end{bmatrix}, \tag{27}$$

in which, β_{ad} and β'_{ad} are the adaptively estimated results, β_{in} and β'_{in} denote the initial value for each. To prevent the filtering divergence, the same limitation has been made for β_{ad} and β'_{ad}. β_{ad} is set within $0 \leq \beta_{ad} \leq 0.5$, β_{in} is supposed as 0.5, β'_{ad} is set within $0 \leq \beta'_{ad} \leq 0.1$ and β'_{in} is set to be 0.1.

Finally, throughout the further limited estimation, the localisation performance can be further improved.

As a summary, to comprehensively describe the operational process of the TC-AEKF based sensor fusion approach, the structure for the algorithm is depicted in Fig. 2. As from the algorithm structure, in comparison with the traditional LC-EKF approach, the further improvement from different perspectives has been made. Firstly, the angular rate is considered in the state prediction process. It is to prevent the performance influence from the potential drift on the attitude information from IMU. Secondly, the approach which can be utilised for the estimation of the two noise covariance matrices is incorporated in the algorithm. With the estimation of these matrices, the adaptive ability of the algorithm can be improved to adapt the changing operational environment. Finally, and most importantly, in order to further limit the estimation of these two noise covariance matrices, two adaptively estimated weighting factors are introduced in the proposed algorithm. With the involvement of these two weighting factors, the potential filtering divergence can be ignored and the performance of the algorithm can be further improved.

IV. Simulation and Experiment

In this section, to quantitatively evaluate the performance of the proposed algorithm and the system, different simulations and experiments have been conducted.

A. Simulation

Before actual experiments, simulations for UAV flight tests in the Gazebo environment have been carried out. Within these, the UAV is deployed in an extremely confined space to mock the actual operational environment. The size of the operational space is set as X: 1.95m, Y: 3.0m and Z: 2.3m. Four fixed anchor nodes are deployed in the localisation area with the coordinates depicted in Fig. 5. Here it needs to note that, in order to mock the extremely confined space where difficult for human to access, all the anchor nodes are mounted on X-Z plane (the X-Z plane is assumed as the entrance of this confined space).

The planned path for UAV in the simulation is set as a rectangle, different algorithms including the TC-EKF, the algorithms in [18], [20] and [21], the TC-AEKF with constant weighting factors, the LC-AEKF from the authors previous work [27] and the proposed approach are simulated. The algorithm in [20] is selected for comparison is under the consideration that it can represent the traditional EKF based sensor fusion UAV localisation approach. The algorithm proposed in [18] is more like an improved version of the traditional approach, which considered the angular rate in the state prediction process. However, the utilisation of the estimated position information as the observation information limits its performance. Most relevantly, the algorithm in [21] considered the angular rate in the state prediction process and took the ranging information as the observation information. This can be the best comparison algorithm to show the adaptive ability of the proposed algorithm. It needs to note that, owing to the unacceptable localisation accuracy (around 30cm, according to the actual experiment) for the single UWB approach in our focused environments, the traditional LC approach is easy to beat approach. Therefore, the LC-AEKF approach considered in the current simulation is the partly LC-AEKF approach which leverages the ranging information for UAV positioning. Since the AEKF based approach is feasible for the application in changing environments, the standard deviation for the measurement noise of the distance information is randomly set within [0,0.2]m in the simulation. The flight test results, including the 3D trajectories, trajectories in three directions, root mean square error (RMSE) in three directions and the empirical cumulative distribution function (eCDF) are depicted in Fig. 3. Meanwhile, the ground truth for each algorithm, which is directly measured by the simulation platform, has also been provided in Fig. 4. Moreover, to make it more intuitive, the detailed information including the localisation median error, 95^{th} percentile error and the average STD for each algorithm have been summarised in Table II. Within these, the numbers behind the TC-AEKF approach are the value for the weighting factors α', α, β' and β, respectively. Before the simulation results analysation, some comments are made here. For the trajectory simulation results, it can be observed that, the offset always exists between the ground truth in Fig. 4 and the planned path. Considering the trajectory results in Fig. 4 are the ground truths, therefore, this offset is only caused by the control model of the UAV in the simulation platform. It has no relationship with the proposed positioning algorithm. As this paper is focused on the UAV positioning technology, thus, more attention will be given to the results comparison between the ground truths and the estimated results from the proposed algorithm, in order to measure the performance of the proposed algorithm.

From the simulation results, it can be observed that due to the changing measurement noise, the first four EKF based approaches with the constant noise covariance matrices always show worse performance when being compared with the AEKF based approaches. Especially, for the EKF based approaches in [20] and [21], due to the changing measurement noise, the unsuitable parameter is calculated for the distance calibration method which directly leads to the performance degradation. However, with the distance calibration and the outlier detection method, the average STD for [20] and [21]

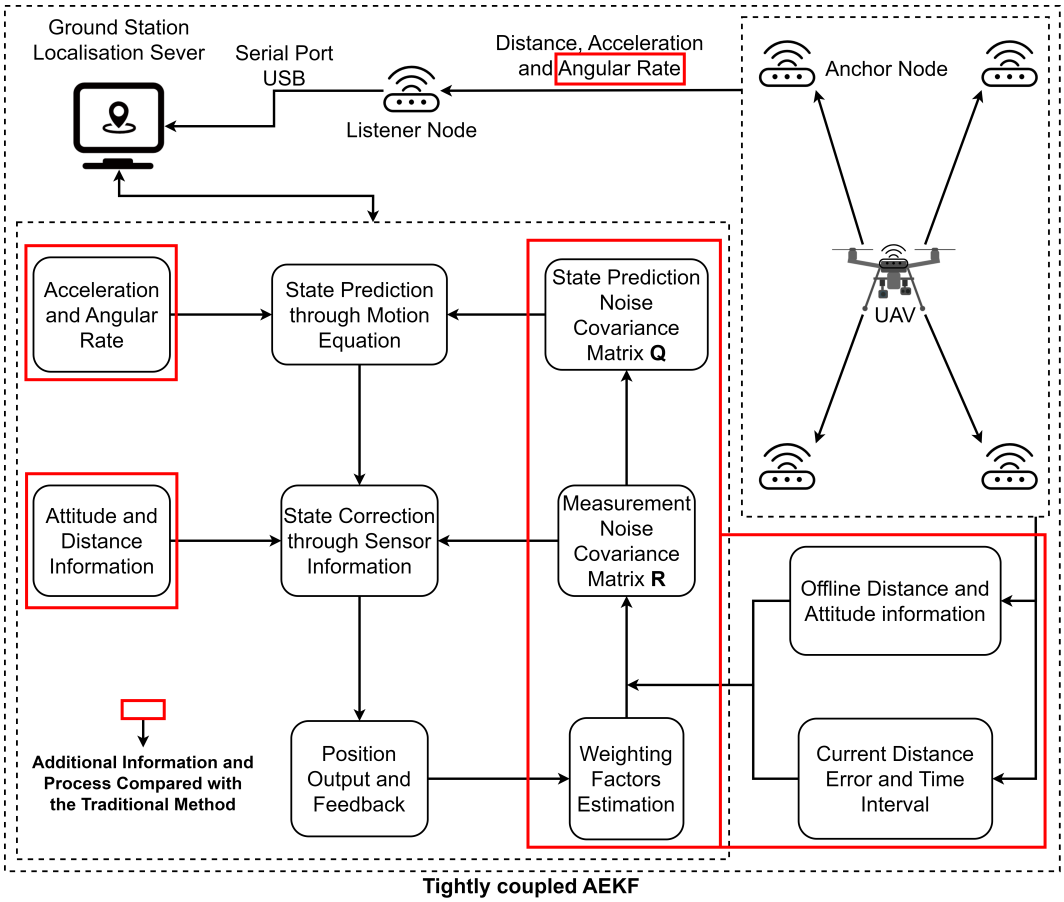

Fig. 2. Algorithm structure.

TABLE II
PERFORMANCE ANALYSIS

	Algorithm	Median Error	Improved	95^{th} Percentile Error	Improved	Average STD	Improved
Simulation	TC-EKF	0.078m	N/A	0.183m	N/A	0.043m	N/A
–	[18]	0.063m	19.2%	0.200m	-9.3%	0.054m	-25.6%
–	[20]	0.117m	-50.0%	0.195m	-6.6%	0.047m	-9.3%
–	[21]	0.088m	-12.8%	0.170m	7.1%	0.042m	2.3%
–	TC-AEKF (0.1, 0.3, 0.1, 0.3)	0.044m	43.6%	0.105m	42.6%	0.027m	37.2%
–	TC-AEKF (0.1, 0.5, 0.1, 0.5)	0.052m	33.3%	0.110m	39.9%	0.030m	30.2%
–	LC-AEKF [27]	0.046m	41.0%	0.125m	31.7%	0.034m	20.9%
–	Our Proposed	0.040m	48.7%	0.099m	45.9%	0.026m	39.5%
Experiment	TC-EKF	0.147m	N/A	0.289m	N/A	0.080m	N/A
–	[18]	0.123m	16.3%	0.275m	4.8%	0.083m	-3.8%
–	[20]	0.183m	-24.5%	0.271m	6.2%	0.068m	15.0%
–	[21]	0.117m	20.4%	0.220m	23.9%	0.051m	36.3%
–	TC-AEKF (0.1, 0.3, 0.1, 0.3)	0.098m	33.3%	0.192m	33.6%	0.044m	45.0%
–	TC-AEKF (0.1, 0.5, 0.1, 0.5)	0.132m	10.2%	0.220m	23.8%	0.049m	38.8%
–	LC-AEKF [27]	0.099m	32.7%	0.180m	37.7%	0.050m	37.5%
–	Our Proposed	0.097m	34.0%	0.167m	42.2%	0.039m	51.3%

can still be improved to 0.047m and 0.042m, respectively. Then, when being focused on the AEKF approaches, through the adaptively estimated noise covariance matrices, the results are significantly smoothed and improved. Clearly, the best performance can be attained through the proposed approach with 0.097m median error, 0.167m 95^{th} percentile error and 0.039m average STD. Meanwhile, compared with the TC-AEKF approach with larger weighting factors ($\alpha = \beta = 0.5$), the one with smaller weighting factors ($\alpha = \beta = 0.3$) holds the better performance. This is relevant to the measurement noise model in the current process, with relatively stable measurement noise model, small weighting factors will get better performance. Furthermore, through the performance comparison between the proposed algorithm and the LC-AEKF, it can be observed that, the median error for these two approaches are almost the same, but the proposed approach shows better performance for the 95^{th} percentile error. However, because the inaccurate attitude information caused by the geomagnetic

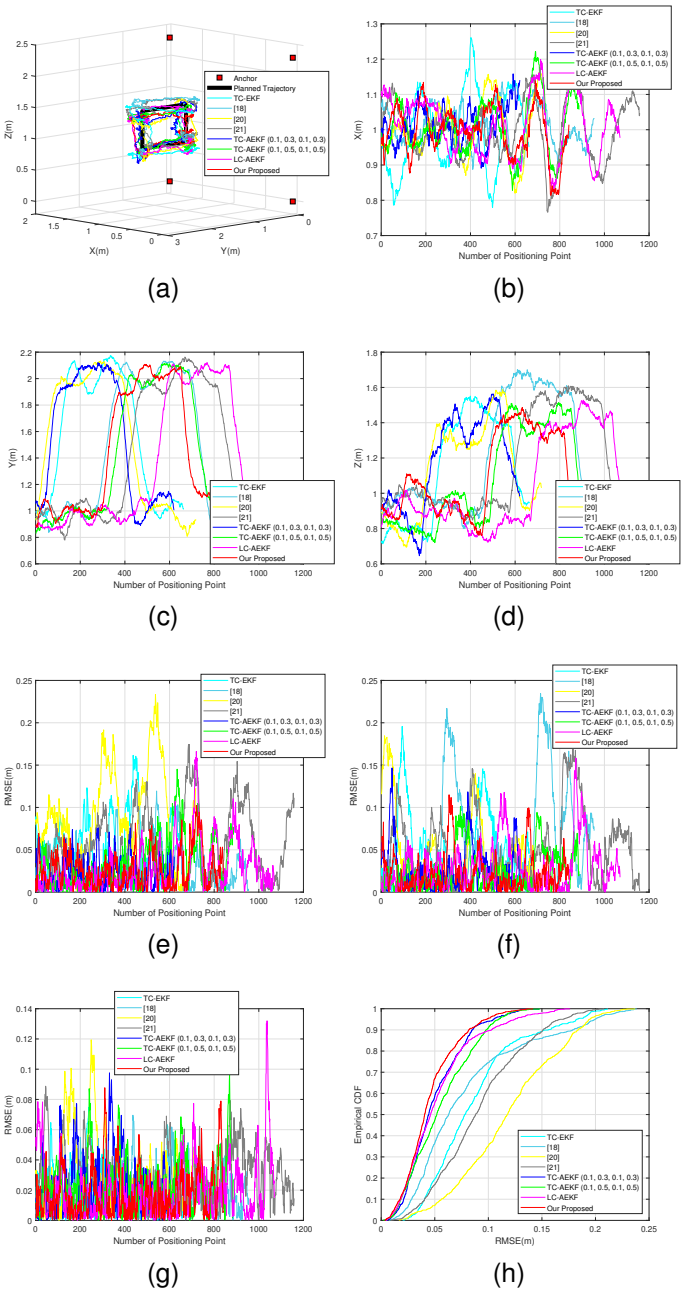

Fig. 3. Simulation results. (a) 3D trajectories. (b) X direction trajectories. (c) Y direction trajectories. (d) Z direction trajectories. (e) X direction RMSE (m). (f) Y direction RMSE (m). (g) Z direction RMSE (m). (h) eCDF.

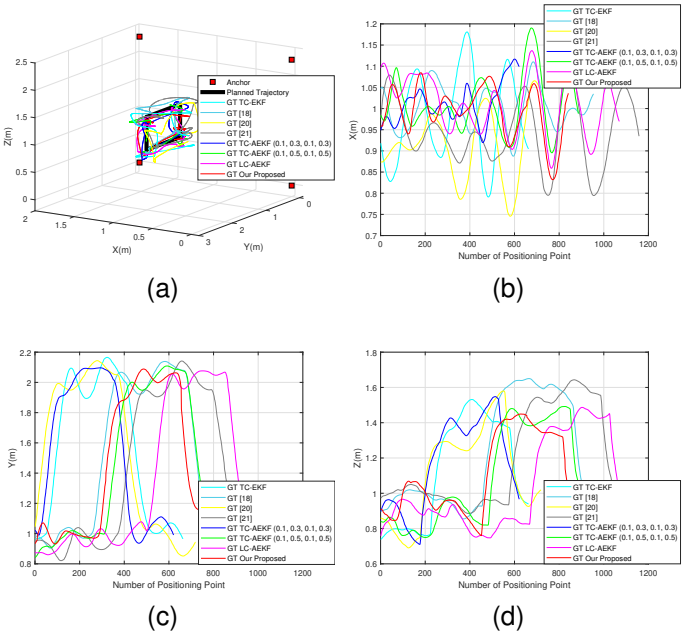

Fig. 4. The ground truth for each algorithm in the simulation (The GT within the figures represents the ground truth). (a) 3D trajectories. (b) X direction trajectories. (c) Y direction trajectories. (d) Z direction trajectories.

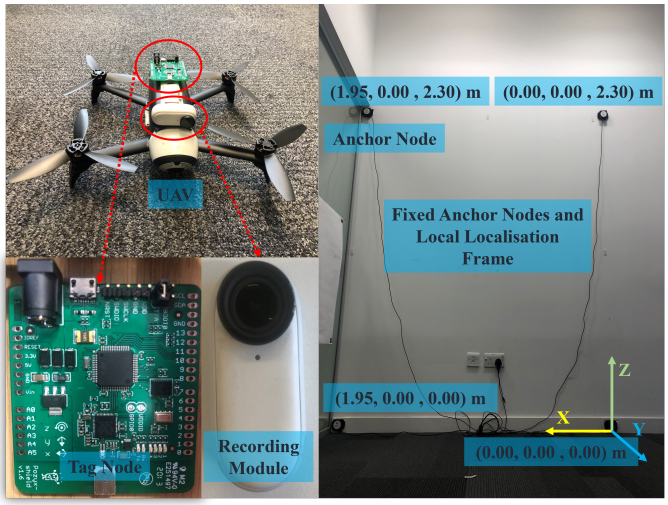

Fig. 5. Experiment environment.

disturbances is difficult to mock in the simulation environment. Therefore, the estimation error of the attitude information is almost the same for these two approaches in the simulation environment.

B. Experiment

1) Experiment configuration: Apart from the simulation, flight tests in the laboratory environment have also been carried out to prove the effectiveness of the proposed algorithm. Same as the simulation, the experiment is performed in an extremely confined space (X: 1.95m, Y: 3.0m, Z: 2.3m) shown in Fig. 5. Clearly, all the fixed anchor nodes have the same coordinates in the simulation, and are mounted on the X-Z plane to mock the human inaccessible environments. The standard deviations for the measurement noise of acceleration, angular rate, attitude and distance information are assumed as 0.5m/s^2, $2.0°$/s, $4.0°$ and 0.1m in the experiment for the non-adaptive algorithms. They are estimated through 1000 recorded information from two IMUs and UWB sensor nodes with the UAV being kept static at the take-off point.

2) Performance evaluation: In the flight tests, the reference system developed by OptiTrack is utilised to serve as the ground truth. The flight path and the evaluated algorithms are the same as in the simulation. In the flight test, the obstacle is used to occlude one of the anchor nodes for a short time period

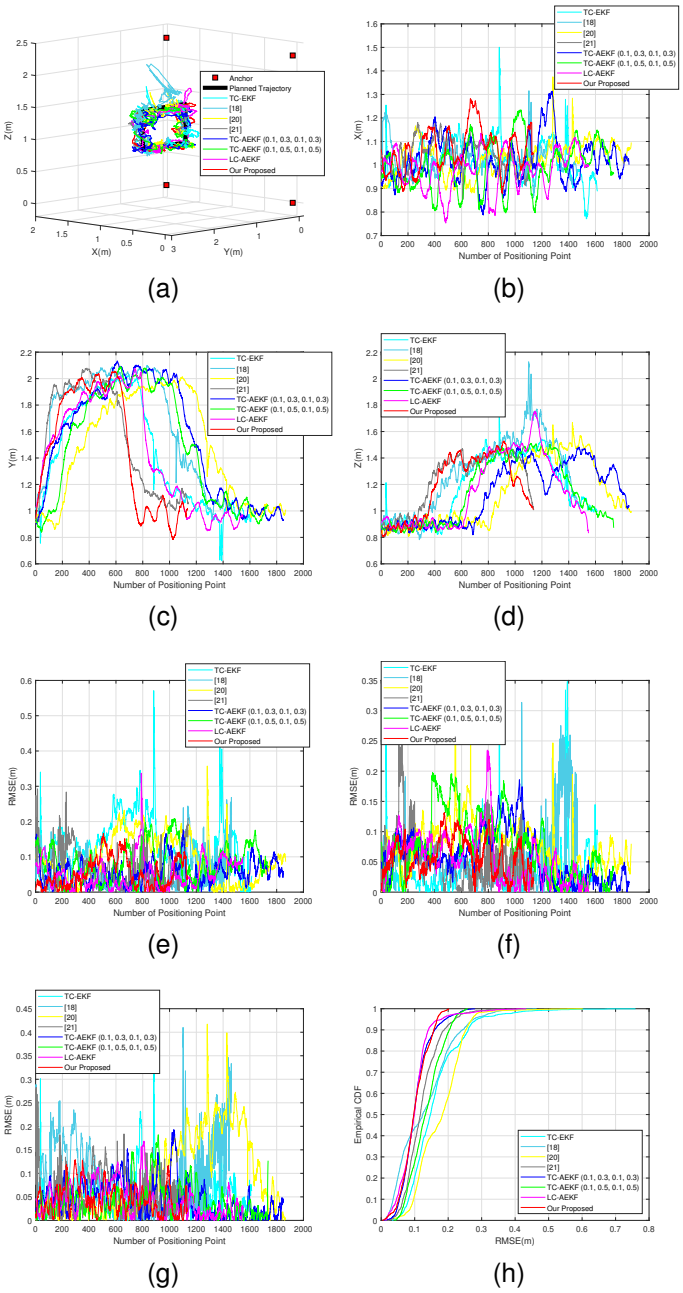

Fig. 6. Experiment results. (a) 3D trajectories. (b) X direction trajectories. (c) Y direction trajectories. (d) Z direction trajectories. (e) X direction RMSE (m). (f) Y direction RMSE (m). (g) Z direction RMSE (m). (h) eCDF.

during the flight to simulate the noise variation environment. The flight test results, the ground truth for each algorithm in the tests, and the detailed performance information are provided in Fig. 6, Fig. 7 and Table II.

Similar to the simulation, the performance gap between the EKF and the AEKF based approaches still exists in the experiment results. But differently, with the suitable calibration parameter, the average STD and accuracy are greatly improved for [20] and [21]. When being focused on the AEKF based approaches, the TC-AEKF approach with smaller weighting factors (0.1, 0.3, 0.1, 0.3) holds the better performance than

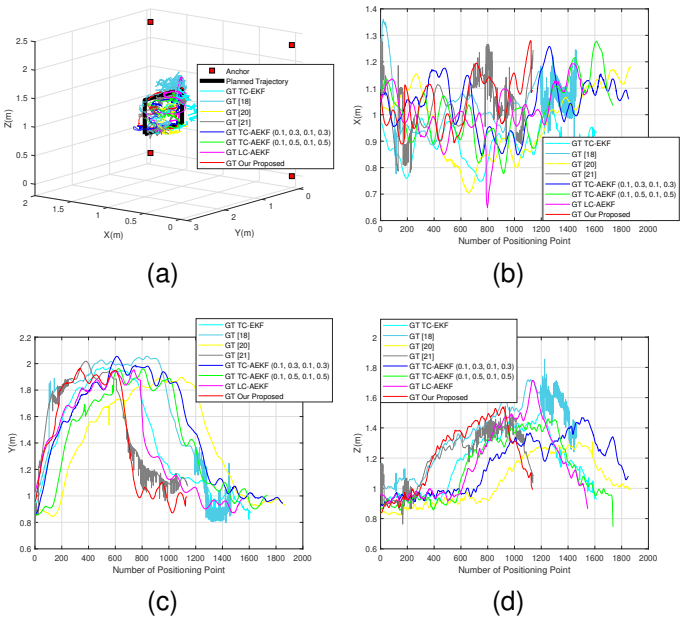

Fig. 7. The ground truth for each algorithm in the experiment (The GT within the figures represents the ground truth). (a) 3D trajectories. (b) X direction trajectories. (c) Y direction trajectories. (d) Z direction trajectories.

the one with relatively larger weighting factors. For the LC-AEKF algorithm, in the actual flight tests, more drift caused by the geomagnetic disturbances for the IMU measurements exist which directly lead to the degradation for the 95^{th} percentile error and the precision (average STD) of the algorithm, the performance oscillation is even larger than the two AEKF approaches with the constant weighting factors. For the proposed approach, it still holds the best performance with the median error, 95^{th} percentile error and average STD to be 0.097m, 0.167m and 0.039m, respectively. In addition to the position estimation, in the actual flight tests, due to the influence from the magnetometer, the drift for the attitude information from the IMU can be observed with the estimation error of the roll, pitch and yaw angle to be 3.06°, 3.71° and 8.78°. Leveraging the proposed approach, this performance degradation is greatly limited with the estimation error to be 2.15°, 1.54° and 4.58°, which are improved 29.8%, 58.4% and 47.8%, respectively.

C. Inspection flight test

Apart from the performance evaluation, in order to comprehensively validate the effectiveness of the proposed algorithm and the developed system, the autonomous inspection flight test in the laboratory environment has been conducted. Apparently, considering the focused application is within the extremely confined environments, the biggest challenge under such circumstance is if the proposed algorithm and the developed system can keep the stability of the UAV and complete the inspection task. Therefore, it is essential to verify the inspection ability with the proposed algorithm and the developed system in the focused environment.

1) Basic setup: For the inspection flight test, the flight area of the UAV is set the same as in the performance evaluation

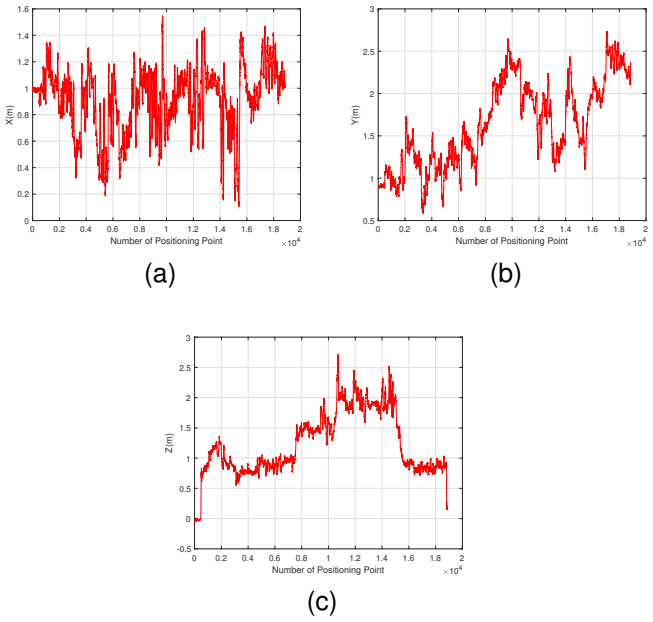

Fig. 8. Flight trajectory for smart inspection. (a) X direction flight trajectory. (b) Y direction flight trajectory. (c) Z direction flight trajectory.

test in the laboratory environment to simulate the extremely confined space (X: 1.95m, Y: 3.0m, Z: 2.3m). The planned flight path for UAV is calculated through the path planning algorithm to cover the whole area for the autonomous inspection. Four anchor nodes are utilised in the system with the same geometry configuration compared with the performance evaluation test. The Insta 360 go 2 is exploited to serve as the recording module for the video recording to do the detailed inspection.

2) Test objective: The objective of this test is to prove that the proposed algorithm together with the developed low cost UAV system is able to do the autonomous inspection in the extremely confined environments. Here it needs to mention that, in this test, taking into account the complexity of the planned path, it is difficult to measure the ground truth during the flight with the existing reference system. Thus, in this test, the reference system is not utilised.

3) Flight test: Considering the aforementioned issue, in the inspection flight test, only the trajectory results from the proposed algorithm are provided in Fig. 8. To make it clearer, the video with the real time trajectory results for the autonomous inspection flight test has been given in URL https://youtu.be/nEgvwbIVRRk. Apparently, the proposed UAV system is capable of the autonomous inspection in extremely confined environments.

V. Conclusion

In this paper, a low cost UAV localisation system with the TC-AEKF based sensor fusion approach is proposed and developed for the autonomous inspection in extremely confined environments. Firstly, the review for the current localisation technologies and systems was presented to illustrate the existing issues. Afterwards, the overview for the system structure and operational process was introduced. To overcome the existing issues, the description for the proposed TC-AEKF based sensor fusion approach was given. With the TC sensor fusion approach and the adaptively estimated noise covariance matrices, the performance of the system was significantly improved. Finally, comprehensive simulations and experiments have been conducted. According to the results, the proposed approach can achieve a high accuracy UAV positioning in focused environments with the median error, 95^{th} percentile error and average STD around 0.097m, 0.0167m and 0.039m, respectively. The estimation error of the roll, pitch and yaw angle was improved to 2.15°, 1.54° and 4.58°. Furthermore, to validate the effectiveness of the proposed system, the autonomous inspection test has been done in the laboratory environment, in order to demonstrate that the developed system with the proposed algorithm is feasible for the autonomous inspection in extremely confined environments.

It still needs to be noticed that the limitation for the proposed algorithm and the system still exists. Currently, with the attached tag nodes on each of the UAVs in the system, it is possible to localise different UAVs simultaneously. However, with the increasing of the tag nodes in the system, the communication burden will also be increased for each of the anchor nodes. This will directly lead to a reduction of the position update rate. Therefore, how to keep the same level position update rate with multiple UAVs exist in the system will be the future research direction. On the other hand, even with the additional weighting factors and the offline data, the performance oscillation and filtering divergence can be limited and avoided. However, this is at the expense of decreasing the adaptive ability and accuracy of the algorithm. Therefore, a new algorithm which can keep the adaptive ability and precision of the system simultaneously is still required. This will be another research direction for us.

References

[1] T. Özaslan, G. Loianno, J. Keller, C. J. Taylor, and V. Kumar, "Spatio-temporally smooth local mapping and state estimation inside generalized cylinders with micro aerial vehicles," *IEEE Robot. Autom. Lett.*, vol. 3, no. 4, pp. 4209–4216, 2018.

[2] M. Petrlík, T. Báča, D. Heřt, M. Vrba, T. Krajník, and M. Saska, "A robust uav system for operations in a constrained environment," *IEEE Robot. Autom. Lett.*, vol. 5, no. 2, pp. 2169–2176, 2020.

[3] P. Tripicchio, M. Satler, M. Unetti, and C. A. Avizzano, "Confined spaces industrial inspection with micro aerial vehicles and laser range finder localization," *Int. J. Micro Air Vehicles*, vol. 10, no. 2, pp. 207–224, 2018.

[4] P. Petráček, V. Krátkỳ, and M. Saska, "Dronument: System for reliable deployment of micro aerial vehicles in dark areas of large historical monuments," *IEEE Robot. Autom. Lett.*, vol. 5, no. 2, pp. 2078–2085, 2020.

[5] Flyability. Elios 2—Indoor Drone for Confined Space Inspections. [Online]. Available: https://www.flyability.com/elios-2

[6] B. Yang and E. Yang, "A survey on radio frequency based precise localisation technology for uav in gps-denied environment," *J. Intell. Robot. Syst.*, vol. 103, no. 3, pp. 1–30, 2021.

[7] A. Couturier and M. A. Akhloufi, "A review on absolute visual localization for uav," *Robot. Auto. Syst.*, vol. 135, p. 103666, 2021.

[8] P. Chhikara, R. Tekchandani, N. Kumar, V. Chamola, and M. Guizani, "Dcnn-ga: A deep neural net architecture for navigation of uav in indoor environment," *IEEE Internet Things J.*, vol. 8, no. 6, pp. 4448–4460, 2020.

[9] Y. Zhou, S. Lai, H. Cheng, A. H. M. Redhwan, P. Wang, J. Zhu, Z. Gao, Z. Ma, Y. Bi, F. Lin *et al.*, "Toward autonomy of micro aerial vehicles in unknown and global positioning system denied environments," *IEEE Trans. Ind. Electron.*, vol. 68, no. 8, pp. 7642–7651, 2020.

[10] J. Qian, K. Chen, Q. Chen, Y. Yang, J. Zhang, and S. Chen, "Robust visual-lidar simultaneous localization and mapping system for uav," *IEEE Geosci. Remote Sens. Lett.*, vol. 19, pp. 1–5, 2021.

[11] Geodetics. Drone Navigation and Photogrammetry. [Online]. Available: https://velodynelidar.com/case-studies/geodetics/

[12] D. Kang and Y.-J. Cha, "Autonomous uavs for structural health monitoring using deep learning and an ultrasonic beacon system with geotagging," *Comput.-Aided Civil Infrastructure Eng.*, vol. 33, no. 10, pp. 885–902, 2018.

[13] Y. Xu, Y. S. Shmaliy, C. K. Ahn, T. Shen, and Y. Zhuang, "Tightly coupled integration of ins and uwb using fixed-lag extended ufir smoothing for quadrotor localization," *IEEE Internet Things J.*, vol. 8, no. 3, pp. 1716–1727, 2020.

[14] S. Kuutti, S. Fallah, K. Katsaros, M. Dianati, F. Mccullough, and A. Mouzakitis, "A survey of the state-of-the-art localization techniques and their potentials for autonomous vehicle applications," *IEEE Internet Things J.*, vol. 5, no. 2, pp. 829–846, 2018.

[15] D. Feng, C. Wang, C. He, Y. Zhuang, and X.-G. Xia, "Kalman-filter-based integration of imu and uwb for high-accuracy indoor positioning and navigation," *IEEE Internet Things J.*, vol. 7, no. 4, pp. 3133–3146, 2020.

[16] B. Yang, E. Yang, L. Yu, and A. Loeliger, "High-precision uwb-based localisation for uav in extremely confined environments," *IEEE Sensors J.*, vol. 22, no. 1, pp. 1020–1029, 2021.

[17] Q. Fan, B. Sun, Y. Sun, and X. Zhuang, "Performance enhancement of mems-based ins/uwb integration for indoor navigation applications," *IEEE Sensors J.*, vol. 17, no. 10, pp. 3116–3130, 2017.

[18] M. Strohmeier, T. Walter, J. Rothe, and S. Montenegro, "Ultra-wideband based pose estimation for small unmanned aerial vehicles," *IEEE Access*, vol. 6, pp. 57 526–57 535, 2018.

[19] S.-G. Kwon, O.-J. Kwon, K.-R. Kwon, and S.-H. Lee, "Uwb and mems imu integrated positioning algorithm for a work-tool tracking system," *Appl. Sci.*, vol. 11, no. 19, p. 8826, 2021.

[20] K. Guo, Z. Qiu, C. Miao, A. H. Zaini, C.-L. Chen, W. Meng, and L. Xie, "Ultra-wideband-based localization for quadcopter navigation," *Unmanned Syst.*, vol. 4, no. 01, pp. 23–34, 2016.

[21] M.-G. Li, H. Zhu, S.-Z. You, and C.-Q. Tang, "Uwb-based localization system aided with inertial sensor for underground coal mine applications," *IEEE Sensors J.*, vol. 20, no. 12, pp. 6652–6669, 2020.

[22] A. Mohamed and K. Schwarz, "Adaptive kalman filtering for ins/gps," *J. Geod.*, vol. 73, no. 4, pp. 193–203, 1999.

[23] F. Jiancheng and Y. Sheng, "Study on innovation adaptive ekf for in-flight alignment of airborne pos," *IEEE Trans. Instrum. Meas.*, vol. 60, no. 4, pp. 1378–1388, 2011.

[24] M. Song, R. Astroza, H. Ebrahimian, B. Moaveni, and C. Papadimitriou, "Adaptive kalman filters for nonlinear finite element model updating," *Mech. Syst. Signal Process.*, vol. 143, p. 106837, 2020.

[25] Y. Huang, Y. Zhang, B. Xu, Z. Wu, and J. A. Chambers, "A new adaptive extended kalman filter for cooperative localization," *IEEE Trans. Aerosp. Electron. Syst.*, vol. 54, no. 1, pp. 353–368, 2017.

[26] Y. Huang, M. Bai, Y. Li, Y. Zhang, and J. Chambers, "An improved variational adaptive kalman filter for cooperative localization," *IEEE Sensors J.*, vol. 21, no. 9, pp. 10 775–10 786, 2021.

[27] B. Yang, E. Yang, L. Yu, and C. Niu, "Adaptive extended kalman filter-based fusion approach for high-precision uav positioning in extremely confined environments," *IEEE/ASME Trans. Mechatronics*, 2022.

[28] A. Benini, A. Mancini, and S. Longhi, "An imu/uwb/vision-based extended kalman filter for mini-uav localization in indoor environment using 802.15. 4a wireless sensor network," *J. Intell. Robot. Syst.*, vol. 70, no. 1, pp. 461–476, 2013.

[29] J. Kelly and G. S. Sukhatme, "Visual-inertial sensor fusion: Localization, mapping and sensor-to-sensor self-calibration," *Int. J. Robot. Res.*, vol. 30, no. 1, pp. 56–79, 2011.

[30] S. Akhlaghi, N. Zhou, and Z. Huang, "Adaptive adjustment of noise covariance in kalman filter for dynamic state estimation," in *Proc. IEEE Power Energy Soc. Gen. Meeting*. IEEE, 2017, pp. 1–5.

Beiya Yang (Member, IEEE) received the B.Eng. degree in Electronic Information Engineering from Northwestern Polytechnical University, Xi'an, China, in 2013 and the M.Sc degree in Information and Communication Engineering from National University of Defense Technology, Changsha, China, in 2015. He received his Ph.D. degree in high-precision positioning technology, from the Department of Design, Manufacturing and Engineering Management (DMEM), University of Strathclyde, Glasgow, UK, in 2023. His current research interests include indoor localisation technology and wireless sensor networks.

Erfu Yang (Senior Member, IEEE) received his Ph.D. degree in Robotics from the School of Computer Science and Electronic Engineering, University of Essex, Colchester, UK, in 2008. He is currently a Senior Lecturer in the Department of Design, Manufacturing and Engineering Management (DMEM), University of Strathclyde, Glasgow, UK. His main research interests include robotics, autonomous systems, mechatronics, manufacturing automation, signal and image processing, computer vision and applications of machine learning and artificial intelligence, etc. He has over 170 publications in these areas, including more than 80 journal papers and 10 book chapters. Dr. Yang has been awarded over 15 research grants as PI (principal investigator) or CI (co-investigator). He is the Fellow of the UK Higher Education Academy, Member of the UK Engineering Professors' Council, Senior Member of the IEEE Society of Robotics and Automation, IEEE Control Systems Society, Publicity Co-Chair of the IEEE UK and Ireland Industry Applications Chapter, Committee Member of the IET SCOTLAND Manufacturing Technical Network. He is also an associate editor for the Cognitive Computation journal published by Springer.

Leijian Yu (Graduate Student Member, IEEE) received the B.Eng. degree in electrical information engineering and the M.Sc degree in information and communication engineering from China University of Petroleum (East China), Qingdao, China, in 2015 and 2018, respectively. He received his Ph.D. degree in robotics and autonomous systems for asset visual inspection, with the Department of Design, Manufacturing and Engineering Management (DMEM) at the University of Strathclyde, Glasgow, UK, in December 2023. His current research interests include machine learning, vision-based autonomous navigation and image contrast enhancement.

Cong Niu (Member, IEEE) has been awarded the B.Eng. with Honours, degree of Electronic Engineering from University of Central Lancashire, Preston, UK in 2014. Then awarded with the M.Sc degree on Embedded Digital System from University of Sussex, Brighton, UK in 2015. He received his Ph.D. degree in robotics and autonomous systems for agriculture applications, from the Department of Design, Manufacturing and Engineering Management (DMEM), University of Strathclyde, Glasgow, UK, in 2021. His current research interests include field and indoor path planning, modeling and simulation, unmanned ground and aerial vehicles and smart factory.